The Effect of Earth-rotation Doppler Shift on SSMIS UAS Channel Measurements

Yong Han

NOAA/NESDIS/Center for Satellite Applications and Research, 5200 Auth Road, Camp Springs, MD 20746, USA

Abstract

The atmospheric radiation near 60 GHz received by the Special Sensor Microwave Imager/Sounder (SSMIS) on board the US Defense Meteorology Satellite Program (DMSP) F-16 satellite exhibits a Doppler shift of up to 75 KHz, due to the Earth's rotation. The magnitude of the Doppler shift varies with the latitude of the observations. Effect of the Doppler shift on the measurements is a function of the Earth magnetic field strength and the angle between the Earth's magnetic field and propagation direction of the electromagnetic wave, which is related to the so called Zeeman-splitting effect. As a result of the frequency shift, the brightness temperatures can differ by 2 K at SSMIS channels 19 – 21. Our analyses also confirm that the SSMIS upper atmosphere sounding channels measure the right-circularly polarized radiation

Introduction

Special Sensor Microwave Imager/Sounder (SSMIS) on board the US Defense Meteorology Satellite Program (DMSP) F-16 satellite includes six upper atmosphere sounding (UAS) channels, channels 19 – 24. These channels have narrow spectral passbands near the line centers of the O_2 magnetic dipole transitions. Their sensitivities peak in the upper stratosphere and mesosphere. Because of Zeeman-splitting, the energy received in some of the UAS channels is partially polarized and depends strongly on the geomagnetic field and its orientation with respect to the propagation direction of the electromagnetic wave. To assimilate measurements from the UAS channels, a radiative transfer (RT) model has been developed for rapid radiance simulations and radiance derivative (Jacobian) calculations, in which the Zeeman-splitting effect has been taken into account [Han et al., 2007]. However, the frequency shift of the radiation spectrum due to the Earth's rotation [Kerola, 2007; Swadley et al., 2008] is ignored in the model.

SSMIS is a conical scanner viewing the Earth at a constant 45^o angle from nadir on a polar orbit with an inclination of 98.8^o and an average orbital altitude of approximately 850 km. Thus, both the satellite orbital motion and the Earth's rotation can result in Doppler shift in the received radiation spectrum. The Doppler component due to the satellite orbital motion has been compensated instrumentally by tuning the frequency of the receiver phase-locked local oscillator as a function of scan angle. This onboard "hardware Doppler" compensation removes the requirement for the RT model to deal the Doppler shift effect when brightness temperatures are calculated and compared to satellite measurements. However, the same measure has not been implemented for the Doppler component due to the Earth's rotation. Kerola [2007] gives an example of the simulated brightness temperature (BT) measurements near the Equator, where the Doppler shift is the largest at certain scan positions, showing the affect of the Earth-rotation Doppler shift is up to a couple of tenths of a degree in Kelvin (K). In our work reported here, an analysis of the Doppler shift effect on a global scale was carried out. The results show that the effect can be as large as 2 K in certain regions and therefore can not be ignored in radiance simulations in these regions.

There has been confusion about whether the measured radiation is left-circularly polarized (LCP) or right-circularly polarized (RCP). The source of the confusion may come from distributed documents which use different conventions to describe the LCP or RCP radiation. For instance, [Kerola, 2007] adopts the physics convention and assumes LCP measurement when modeling the deviation of measurements from the desired values due to antenna system axial ratios departure from unity. However, the report [Poe et al., 2001] describes the measured radiation is RCP. Another possible source of the confusion is that the polarization specification can be made for a radiometer system which may or may not include the reflector that directs

the incoming radiation to the receivers. The reflector reverses the polarization. As a result, the RCP radiation is actually measured with an LCP radiometer and vise versa. It will be explained later that the polarization issue is not important if there is no frequency shift in the radiation spectrum, because an LCP system will receive approximately the same amount of energy as an RCP system. But it becomes important if the frequency shift has a measurable effect. In this paper, the Institute of Electrical Engineers convention is used, which is the opposite of the physics convention, and the reflector is assumed to be included in the radiometer system.

The impact of the Doppler-shift predicted from theory

It is not straightforward to observe the Doppler-shift effect in the measurements, because the variations from other factors such as the Earth's magnetic field ***Be*** and the angle θ_B between ***Be*** and the wave propagation direction ***k*** may dominate the features in the received signals. To isolate the Doppler-shift effect, we first conducted a theoretical analysis by simulating radiance measurements.

Radiance simulation

In the upper stratosphere and mesosphere, the O_2 transition lines are narrow, and the Zeeman splitting may become an important factor in the RT modeling [Lenoir, 1968]. Each line splits into three groups of sublines, usually referred as the π, σ+ or σ- components. The spread width of the sublines is on the order of $0.05Be$ MHz, where Be is the magnitude of ***Be***, which may take a value in the range of 23 – 65μT near the Earth surface. Thus, the Zeeman splitting effect may be observed by a space-based sensor only with narrow passbands near the centers of the unsplit transition lines. As listed in Table 1, SSMIS channels 19 and 20 have passbands centered on the transition lines, designated as 7+, 9+, 15+ and 17+ [Rosenkranz, 1993], with passband widths about 1 MHz, and therefore are strongly influenced by the Zeeman effect. The other four channels each have four passbands, paired and situated symmetrically on opposite sides of the transition lines 7+ or 9+ with increased bandwidths and band frequency-offsets from the line centers as the channel number increases. Thus their sensitivity to the Zeeman effect decreases with the channel number. For channels 23 and 24, the Zeeman effect is negligible.

In a circular polarization basis, the spectral intensity of thermal microwave radiation may be expressed by the BT coherent matrix, as

$$T_{b,\nu} = \begin{bmatrix} T_{b,r,\nu} & T_{b,rl,\nu} \\ T*_{b,rl,\nu} & T_{b,l,\nu} \end{bmatrix} \quad (1)$$

where $T_{b,r,,\nu}$ and $T_{b,l,,\nu}$ are respectively the RCP and LCP components, $T_{b,rl,,\nu}$ is the coherency (the symbol * represents complex conjugate) and ν is the frequency. The solution solving the radiative transfer equation for $T_{b,,\nu}$ at the top of atmosphere (TOA) is given in [Rosenkranz and Staelin, 1988]. The simulation of the radiance measurement or channel BT, labeled here as $T_{b,ch}$, is performed by convolving $T_{b,\nu}$ with the channel's spectral response function (SRF). Both $T_{b,,\nu}$ and $T_{b,ch}$ are a function of air temperature T_{air}, Be and $\cos(\theta_B)$.

When there is a Doppler-shift $\Delta\nu$ in the incoming radiation spectrum, $T_{b,ch}$ also depends on $\Delta\nu$. Moreover, the characteristics of the dependence are different between RCP and LCP systems. Figure 1 shows an example of $T_{b,r,\nu}$ and $T_{b,l,\nu}$ spectra near the 9+ line, computed for the US 76 standard atmosphere at Be = 50μT and three values of θ_B (0, 90° and 180°). It can be seen that the spectra of $T_{b,r,\nu}$ and $T_{b,l,\nu}$ are in mirror symmetry, that is, $T_{b,r,\nu}$ at ν- ν_0 is the same as $T_{b,l,\nu}$ at ν_0-ν, where ν_0 is the center of the unsplit line. This property may be proved by applying Theorem 3 and equation 45 in [Stogryn, 1989] and holds in general at other values of Be and θ_B near the line center $\nu_{0,}$ where the contributions from other lines may be ignored. The property implies that the LCP and RCP systems with symmetrical passbands would receive the same amount of energy if there is no frequency shift in the radiation spectrum. However, if the spectrum is shifted, the two systems would in general receive a different amount of energy if $\theta_B \neq 90°$. For example, the passbands of channels 19 and 20 are centered on the transition lines, and it can be seen from Figure 1 that a small positive frequency shift of the spectrum (add a constant to the spectral frequency) would increase

(decrease) $T_{b,r,ch}$ but decrease (increase) $T_{b,l,ch}$ at $\theta_B > 90^o$ ($\theta_B < 90^o$). The situation is reversed for a small negative frequency shift. At $\theta_B = 90^o$, the three Zeeman components are all linear polarized and the LCP and RCP systems would observe the same radiance. Notice also that the curves for $\theta_B = 90^o$ in Figure 1 are quite flat near the center of the line, implying that the variation due to the Doppler-shift would be small under this condition.

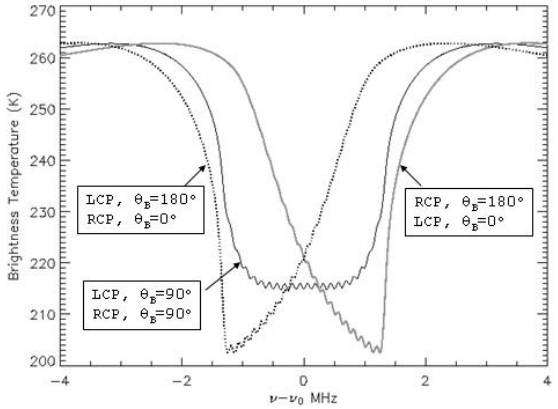

Figure 1. A brightness temperature spectrum near the 9+ transition line centered at v_0 = 61.150560 GHz, for the US 76 standard atmosphere and *Be* = 50 μT. Note that the curve for the right-circularly polarization (RCP) at θ_B is identical with that for the left-circularly polarization (LCP) at 180^o- θ_B.

Table 1. SSMIS UAS channel parameters. Offset – passband central frequency offset from the unsplit O_2 transition line center; BW – bandwidth. The line centers of the transitions, represented with 7+, 9+, 15+ and 17+, are 60.434776, 61.150560, 62.997977 and 63.568518 GHz, respectively.

Ch	Passband 1		Passband 2		Passband 3		Passband 4		NEΔT (K)
	Offset (MHz)	BW (MHz)	Offset (MHz)	BW (MHz)	Offset (MHz)	BW (MHz)	Offset (MHz)	BW (MHz)	
19	0 (15+)	1.34	0 (17+)	1.36					1.76
20	0 (7+)	1.34	0 (9+)	1.37					1.80
21	-2 (7+)	1.26	2 (7+)	1.23	-2 (9+)	1.33	2 (9+)	1.33	1.27
22	-5.5 (7+)	2.62	5.5 (7+)	2.61	-5.5 (9+)	2.66	5.5 (9+)	2.67	0.70
23	-16 (7+)	7.01	16 (7+)	7.17	-16 (9+)	7.40	16 (9+)	7.44	0.43
24	-50 (7+)	26.63	50 (7+)	26.33	-50 (9+)	26.04	50 (9+)	26.88	0.44

Doppler shift due to Earth's rotation

The radial velocity of the radiation emitters due to the Earth's rotation at a given direction $\boldsymbol{k}$ is independent of the distance between the emitters and satellite, and the Doppler frequency shift Δν is given by [Swadley et al., 2008] and is written here in a slightly different form, as

$$\Delta\nu = -\frac{\overline{\nu}}{c}\Omega R_s \cos(\psi)[\cos(i)\cos(\varphi) \pm \sin(\varphi)\sqrt{\sin(i-\lambda)\sin(i+\lambda)}] \quad (2)$$

where $\overline{\nu}$ is the mean frequency of the channel passbands, c is the speed of light, Ω is the angular velocity of the Earth's rotation, R_s is the distance of the satellite from the center of the Earth, ψ is the viewing angle from nadir, i is the inclination of the orbit, λ is the latitude (positive in Northern Hemisphere, negative in Southern Hemisphere and zero at Equator) of the satellite nadir point, and φ is the scan angle from the satellite orbital motion direction. The scan angle φ is related to the scan position j, as

$$\varphi = (\frac{1}{2} - \frac{j-1}{N-1})\Gamma, \quad j = 1, N \quad (3)$$

where N (=30) is the number of scan positions and Γ is the total scan angle between scan positions 1 and N. Scan position 1 corresponds to the east-most pixel in each scan data set for the ascending observations and west-most for the descending observations. The plus and minus signs before the second term in (2) correspond to the ascending and descending orbits, respectively. The first term in (2) is due to the departure of i from 90^o and is a positive contribution at φ=0^o, since $\boldsymbol{k}$ has a component to the East at this angle. The second term is due to an angle from the North and is zero at φ=0^o. The shift may reach 75 KHz in the tropical region at the edges of the scans.

The dependence of the Doppler-shift effect on *Be* and θ_B

The effect of the Doppler-shift in the range computed with (2) is first evaluated by comparing simulated brightness temperatures with and without the inclusion of a frequency shift. The simulations use temperature profiles from the empirical model, COSPAR International Reference Atmosphere [Fleming et al. 1988] (CIRA-88). The lower part (0 – 120 km) of the model profile includes monthly values of the temperature field on the latitude grid points with a 5-degree interval from 80°N to 80°S, generated from data including ground-based and satellite measurements. Figure 2 shows the BT differences, BT(Δν)-BT(Δν=0), for channels 19-22 as a function of the frequency shift, calculated at three values of cos(θ_B) (-1, 0,1). Figure 2a and 2b are for RCP and LCP radiometer systems, respectively, with the calculations conditioned at *Be* =30 μT. Figure 2c is for an RCP system with *Be* =60 μT (The figure for an LCP system is not shown since the pattern is similar to Figure 2b). It can be seen that for channels 19 and 20, the BT differences can reach a value of about 2 K when cos(θ_B) is near 1 or -1, and become small when cos(θ_B) is near zero. The BT differences for an RCP system are almost opposite to those for an LCP system, which is consistent with the mirror symmetric property of the spectrum discussed in the previous section. The dependence of the BT differences on *Be* is larger for smaller *Be*, since the width of the Zeeman-splitting (see Figure 1) becomes narrower for smaller *Be*, resulting in a larger sensitivity to the Doppler-shift. Small *Be* occurs near Equator (see Figure 5), which may coincide with large Doppler-shifts. The temperature profile used in the calculations for Figure 2 is an annual mean at 17^{o}N. Hence we emphasize that the magnitude of the BT difference also depends on the temperature lapse rate of the portion of the atmosphere which the channels are sensitive to. As the frequency of the radiation spectrum is shifted, the peak height of the channel's weighting function (WF) may shift up or down accordingly, resulting in a decrease or increase of the amount of BT depending on the temperature lapse rate. For channel 21, the BT differences are relatively small, and the sign of the differences are opposite to those in channels 19 and 20, mainly due to the differences in their passbands' spectral locations. For channel 22, as well as channels 23 and 24, the effect of the frequency shift is negligible.

To evaluate the Doppler-shift effect on a global scale, we simulated the measurements of channel 20 for the full day of January 1, 2006. The result is shown in Figure 3a for ascending orbit and Figure 3b for descending orbit, plotted as BT differences between the simulations with and without the inclusion of the effect of the Earth's rotation. The corresponding data for the simulations, including *Be* and |cos(θ_B)| (the absolute value of cos(θ_B)), are taken from the SSMIS Sensor Data Records (SDRs). The signs of the cos(θ_B) data, not included in SDRs, were derived with the help of the 10th International Goemagnetic Reference Field (IGRF) model [Mandea et al., 2000]. It can be seen from the figures that the BT differences can be as large as 2K, but not necessarily occur in the tropical region, where the tangent velocity of the Earth's rotation is the largest, because of the dependence of the effect on the angle θ_B discussed earlier. To discuss it further, the corresponding cos(θ_B) and *Be* data are plotted and shown in Figure 4 and 5, respectively. It can be seen that the BT differences are large at the pixel positions where the Doppler-shifts are large and the values of |cos(θ_B)| are close to 1. They become small in high latitudes, where Dopper shifts are small, and in regions where the values of cos(θ_B) are near zero ($\theta_B \approx 90^o$). Note also the difference of the patterns of the BT differences between the ascending and descending orbits, which is in large degree due to the differences of the angle θ_B between the two sets of data. Finally we observe from the cos(θ_B) images that between 10^{o}N and 40^{o}N from the ascending observations and -40^{o}S and 0^o from the descending observations, there are

pixels in the same scan on which the values of cos(θ_B) on the east and west sides with respect to the ground track are approximately the same and close to -1 or 1, and the signs of Δν are opposite between the two sides. This feature provides a way to evaluate the Doppler-shift effect in the measurements.

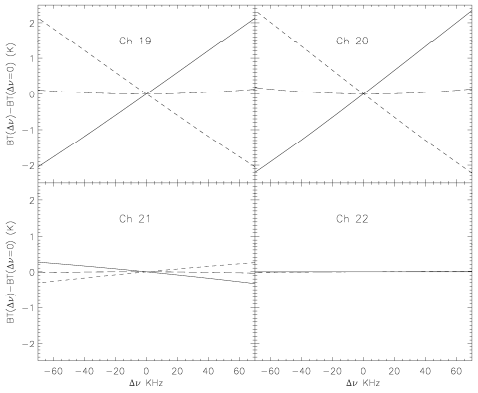

Figure 2a

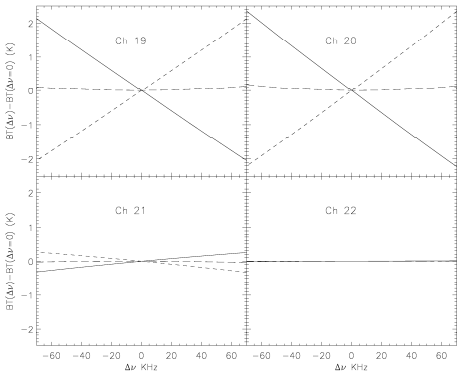

Figure 2b

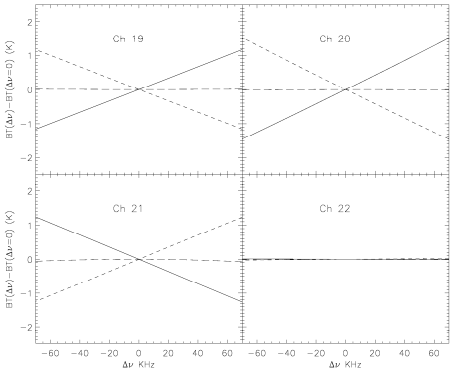

Figure 2c

Figure 2. Simulated brightness temperature (BT) differences using the RT models with and without the inclusion of the Doppler-shift effect, with the solid, long-dashed and short-dashed curves corresponding to cos(θ_B) = -1, 0, 1, respectively. (a) *Be* = 30 μT and an RCP radiometer system, (b) *Be* = 30 μT and LCP, and (c) *Be* = 60 μT and RCP.

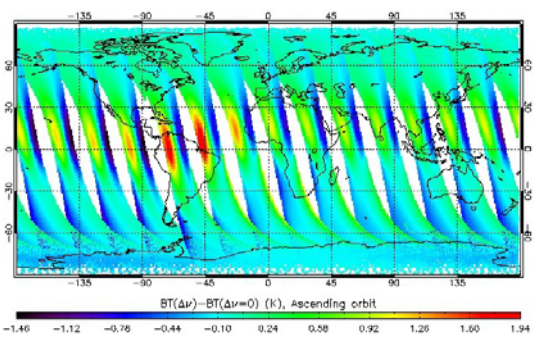

Figure 3a

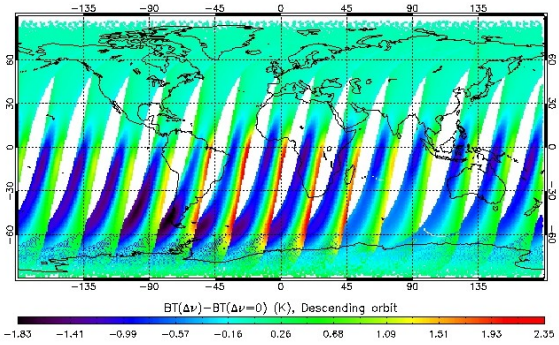

Figure 3b

Figure 3. Simulated brightness temperature (BT) differences for channel 20 using the RT models with and without the inclusion of the Doppler shift effect, for ascending (a) and descending (b) observations on January 1, 2006. For the simulations, the pixel's geometric parameters, *Be* and |cos(θ_B)|, are taken from the SDRs and the temperature profiles are from the CIRA-88 model. The signs of the cos(θ_B) data are recovered with the assistance of the IGRF model.

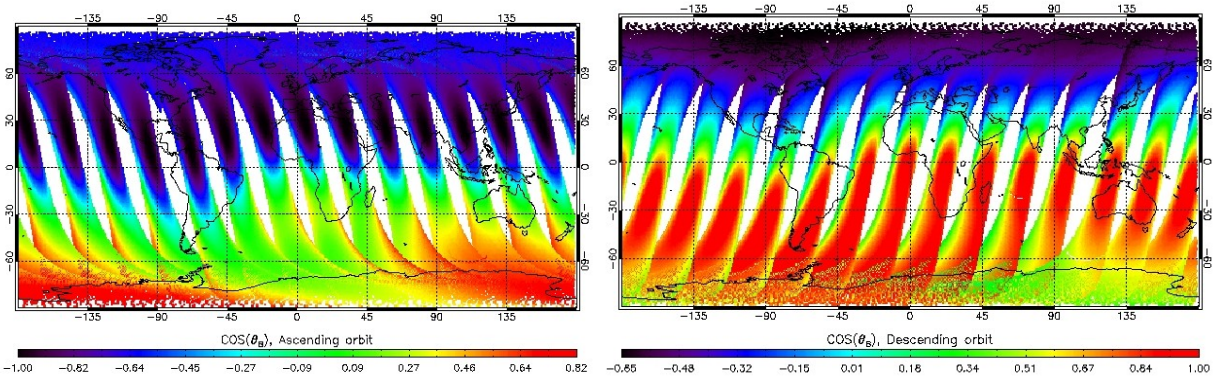

Figure 4a Figure 4b

Figure 4. The cosine of the angle between the magnetic field and wave propagation direction for the ascending (a) and descending (b) observations on January 1, 2006.

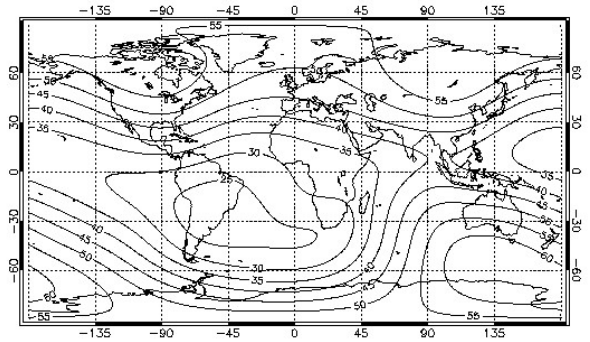

Figure 5. The Earth's magnetic field strength in μT at 00:00 Greenwich Mean Time on January 1, 2006 at the height of 60 km, computed using the IGRF model

Observations of the Doppler-shift effect

As discussed earlier, the BTs in channels 19 – 21 vary with Be, $\cos(\theta_B)$, T_{air} and $\Delta\nu$. Thus, efforts were made to minimize the variations due to the first three factors. The variation due to T_{air} was minimized by averaging data over different locations and a long period of time. To minimize the variations due to Be and $\cos(\theta_B)$ and at the same time maximize the Doppler-shift effect, data were selected from the pixels at the edges of the scans with $|\cos(\theta_B)|$ close to 1 and minimal differences in both Be and $\cos(\theta_B)$ between the data points on the east and west sides of the scans. Specifically, the data selection criteria are the following. The latitudes of the data are confined between 10°N and 40°N for the ascending orbits and between -40°S and 0° for the descending orbits. The reason for such a selection has been discussed in the previous sections. These data were further filtered by selecting data with the absolute values of $\Delta\nu$ to be greater than 55 KHz and the variations in Be and $|\cos(\theta_B)|$ are less than 1 μT and 0.01, respectively. Finally, the data points on the east and west sides of the same scan were paired according to the smallest difference in $\cos(\theta_B)$. The BT differences, BT(west point) – BT(east point), were then computed for each pair of the data points. Note that the Doppler shift is positive on the west data points and negative on the east data points.

The set of data meeting the above criteria were collected from the SDRs in the period of the entire year of 2006, which include 41772 pairs of data samples from ascending orbits and 65476 pairs from descending orbits. The Root-Mean-Square (RMS) differences in Be and $\cos(\theta_B)$ between the paired data points are 0.6 μT and 0.006, respectively, for both the ascending and descending data. The mean values and standard deviations of Be, $\cos(\theta_B)$, $\Delta\nu$ and scan positions of the data set are summarized in Table 2. As listed in the table, the values of $|\cos(\theta_B)|$ in the data set are about 0.7, which are the highest value we can obtain for such paired data in order to maximize the Doppler-shift effect and in the meantime minimize the influence from

other factors. The BT differences between the paired data points are plotted as histograms shown in Figure 6, with the solid curves for ascending observations and dashed curves for descending observations. The corresponding mean values and standard deviations of the BT differences are listed in Table 3 in the rows labeled "Measured". The results show that for channels 19 and 20, there is a positive mean BT difference of about 2 K for the ascending set of data whose $\cos(\theta_B)$ values are negative, and a negative difference of approximately the same magnitude from the descending data whose $\cos(\theta_B)$ values are positive. For channel 21, the BT differences are relatively small but the signs are opposite to those for channels 19 and 20. Since, as mentioned earlier, Δv is negative on the east edge and positive on the west edge, of the scans, this pattern of the BT differences in channels 19 – 21 is consistent with the analysis given in Section 2 and is matched to that of an RCP system. The BT differences for channels 22-24 are small, as expected since the Doppler-shift effect is negligible in these channels.

More insights about the above results may be gained by simulating the BT differences for the same data set. The CIRA-88 model was used to provide the temperature profiles for the simulations. Three sets of simulations were performed. The first two are for RCP and LCP systems, respectively, and the third for an RCP system but without the inclusion of the Doppler-shift. The statistics of the simulations are listed also in Table 3. It can be seen that within the uncertainties in the measurements and model temperature profiles, the effect of the Doppler-shift seen in the measurements agree with that predicted from the theory. Moreover, the measured radiation is clearly not LCP because the signs of the simulated BT differences in channels 19 – 21 under the LCP assumption are opposite to those observed in the measurements. Finally, it is noted that the widths (standard deviations) of the measured BT differences are larger than the simulations, but they decrease with the channel number. One cause for the large widths is likely related to the instrument noise as suggested by the instrument noise levels listed in Table 1. Another possible cause is the variations of the temperature profiles, which are not possible to be taken into account fully in the simulations with the CIRA-88 profile model.

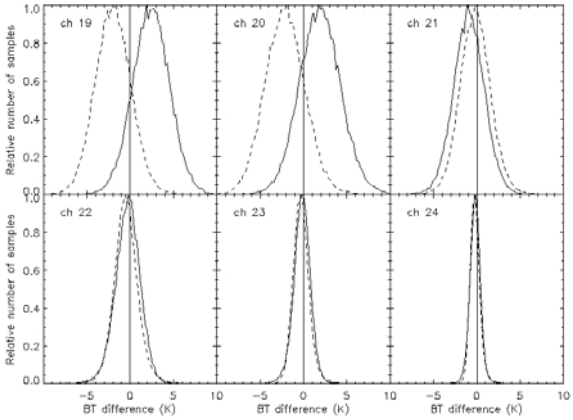

Figure 6. The histograms of the differences of the measured brightness temperature (BT) between the paired data points on the east and west edges of the scans, BT(west) – BT(east), with the solid curves from the ascending observations (sample size = 41772) and the dashed curves from the descending observations (sample size = 65476).

Table 2. Means (the first numbers) and standard deviations (the second numbers) of the Earth's magnetic field strength *Be*, cosine of the angle between the magnetic field and the wave propagation direction $\cos(\theta_B)$, Doppler frequency shift Δv and pixel position, over the data set of *n* samples corresponding to the results in Table 3 and Figure 6. The words "East" and "West" refer to the data pixel positions on the east and west edges of the scans, which containing 30 pixel positions (1 – 30), numbered sequentially from east to west for ascending orbits and west to east for descending orbits.

	Be (μT)	$\cos(\theta_B)$	East Δv (KHz)	West Δv (KHz)	East position	West position
Ascending (n=41772)	41.3, 4	-0.66, 0.05	-62.2, 3.2	65.3, 4.5	2, 1	26, 2
Descending (n=65476)	45.3, 7	0.68, 0.06	-63.0, 3.8	67.4, 4.7	29, 1	4, 2

Table 3. Means (the first numbers) and standard deviations (the second numbers) of the brightness temperature (BT) differences between the paired data points on the east and west edges of the scans, BT(West) – BT(East). The words "Measured" and "simulated" refer to the measured and simulated data, respectively, and "RCP" and "LCP" refer to the radiometer systems with right-circularly and left-circularly polarizations, respectively. The issue of polarization is not important in the simulations with no Doppler shift ($\Delta v=0$).

	Chan 19	Chan 20	Chan 21	Chan 22	Chan 23	Chan 24
Ascending orbit (n=41772)						
Measured	2.54, 2.14	2.03, 2.40	-0.72, 1.38	-0.14, 1.49	-0.05, 1.01	-0.07, 0.68
Simulated RCP	1.76, 0.38	1.65, 0.37	-0.61, 0.28	0.02, 0.22	0.04, 0.23	0.02, 0.14
Simulated LCP	-1.71, 0.32	-1.67, 0.31	0.65, 0.21	0.06, 0.22	0.03, 0.23	0.02, 0.14
Simulated $\Delta v=0$	0.02, 0.24	-0.01, 0.23	0.04, 0.20	0.02, 0.22	0.04, 0.23	0.02, 0.14
Descending orbit (n=65476)						
Measured	-1.84, 2.08	-2.02, 2.32	0.01, 1.80	-0.26, 1.45	-0.14, 0.97	-0.05, 0.65
Simulated RCP	-1.62, 0.41	-1.66, 0.43	0.95, 0.35	0.15, 0.35	0.14, 0.40	0.03, 0.25
Simulated LCP	1.94, 0.46	1.72, 0.54	-1.01, 0.41	0.10, 0.35	0.14, 0.40	0.03, 0.25
Simulated $\Delta v=0$	0.16, 0.26	0.03, 0.34	0.01, 0.18	0.15, 0.35	0.14, 0.40	0.03, 0.25

Conclusions and remarks

The Doppler-shift in the radiation spectrum due to the Earths' rotation can have an effect of up to 2 K on the BT simulations for SSMIS channels 19 – 21. The degree of the effect depends on not only the amount of shift Δv, but also $\cos(\theta_B)$ and *Be* as well as T_{air}. The value of Δv may be calculated with (2). The magnitude of Δv is about 75 KHz near Equator at the pixels on the edges of the scans and decreases with latitude. However, the largest impact of the Doppler-shift does not necessary occur near Equator because of the dependence on $\cos(\theta_B)$. The effect can be large if $|\Delta v|$ and $|\cos(\theta_B)|$ are large and *Be* is small, and become small if $\cos(\theta_B)$ is near zero. *Be* is usually small in low latitudes, but $\cos(\theta_B)$ can vary significantly in these regions. The effect of the Doppler-shift may be neglected at high latitudes in the radiance simulation. For channels 22 – 24, the effect of the Doppler-shift is insignificant. Our analyses also confirm the measured radiation in the UAS channels is RCP

Recently, the fast RT model [Han et al., 2007] has been improved to take the Doppler shift effect into account. However, operational applications of the model require two additional parameters to be included in the SDRs. One is the Doppler-shift Δv and the other is the sign of $\cos(\theta_B)$. The SDR data used in this study include only the absolute value of $\cos(\theta_B)$. As shown in this paper, the sign becomes important if there is a significant Doppler-shift in the radiation spectrum.

References

Han, Y., F. Weng, Q. Liu, and P. van Delst (2007), A Fast Radiative Transfer Model for SSMIS Upper-atmosphere Sounding Channels, *J. Geophys. Res*., 112(D11121), 1468, doi:10,1029/ 2006JD008208.

Kerola, D. X. (2006), Calibration of Special Sensor Microwave Imager/Sounder (SSMIS) upper air brightness temperature measurements using a comprehensive radiative transfer model, *Radio Sci.*, 41, RS4001, doi:1029/2005RS003329**.**

Lenoir, W. B. (1968), Microwave spectrum of molecular oxygen in the mesosphere, *J. Geophys. Res.* 73, 361-376.

Mandea M., S. Macmillan, T. Bondar, V. Golovkov, B. Langlais, F. Lowes, N. Olsen, J. Quinn, and T. Sabaka (2000), International geomagnetic reference field - 2000, *Phys. Earth Plan. Int.*, 120, 39-42.

Poe, G. A., K. Germain, J. Bobak, S. Swadley, J. Wessel, B. Thomas, J. Wang, B. Burns, DMSP Calibration/Validation Plan for the Special Sensor Microwave Imager Sounder (SSMIS), ch. 1, pp. 1- 32, 2001.

Rosenkranz, P. W. and D. H. Staelin (1988), Polarized thermal microwave emission from oxygen in the mesosphere, *Radio Science*, 23, 721-729.

Stogryn, A. (1989), The magnetic field dependence of brightness temperature at frequencies near the O_2 microwave absorption lines, *IEEE Transactions on Geoscience and Remote Sensing*, 27, 279-289.

Swadley S., G. A. Poe, W. Bell, Y. Hong, D. Kunkee, S. McDermid and T. Leblanc (2008), Analysis and Characterization of the SSMIS Upper Atmosphere Sounding Channel Measurements, IEEE Trans. Geosci. And Remote Sensing, SSMIS Special Issue, *IEEE Transactions on Geoscience and Remote Sensing*, 46, 962-983.